Chiral Phonon Transport Induced by Topological Magnons

Even Thingstad, Akashdeep Kamra, Arne Brataas, and Asle Sudbø*
Center for Quantum Spintronics, Department of Physics, Norwegian University of Science and Technology, NO-7491 Trondheim, Norway

(Received 9 August 2018; revised manuscript received 19 December 2018; published 11 March 2019)

The plethora of recent discoveries in the field of topological electronic insulators has inspired a search for boson systems with similar properties. There are predictions that ferromagnets on a two-dimensional honeycomb lattice may host chiral edge magnons. In such systems, we theoretically study how magnons and phonons couple. We find topological magnon polarons around the avoided crossings between phonons and topological magnons. Exploiting this feature along with our finding of Rayleigh-like edge phonons in armchair ribbons, we demonstrate the existence of chiral edge modes with a phononic character. We predict that these modes mediate a chirality in the coherent phonon response and suggest measuring this effect via elastic transducers. These findings reveal a possible approach towards heat management in future devices.

DOI: 10.1103/PhysRevLett.122.107201

Introduction.—Topological electronic insulators [1–5] are characterized by an insulating bulk with conducting "chiral" edge states. The unidirectional propagation of these chiral modes is "topologically protected" against defects at low temperatures when we can disregard inelastic scattering from phonons [5]. This has led to the development of a wide range of essential concepts, including Majorana modes [6–9], topological quantum computation [10,11], and chiral transport. Inspired by these findings, there has been an upsurge of efforts towards finding similar states in other systems [12] with an emphasis on bosonic excitations [13–19]. There are predictions of topological magnons [15–17] in honeycomb ferromagnets with an engineered Dzyaloshinskii-Moriya interaction [20,21] that induces the necessary band gap. In contrast to fermionic systems with Fermi energy within this band gap, the bulk is not necessarily insulating in bosonic systems [22].

The field of magnonics [23–26] focuses on pure spin transport mediated by magnons [27]. It is possible to exploit the low-dissipation and wavelike nature of these excitations in information processing [28,29]. The coherent pumping of chiral surface spin wave (Damon-Eshbach) modes induces cooling via incoherent magnon-phonon scattering [30]. Besides application oriented properties, the bosonic nature of magnons, combined with spintronic manipulation techniques [24,31], allows for intriguing physics [32–35]. The coupling [36] between magnons and phonons fundamentally differs from the electron-phonon interaction and results in a coherent hybridization of the modes [37], in addition to the temperature dependent incoherent effects [30,38] discussed above. The direct influence of the hybridization between magnons and phonons, known as magnon polarons [39,40], has been observed in spin and energy transport in magnetic systems [41–46].

In this Letter, we address the robustness of the topological magnons in a honeycomb ferromagnet [15–17] against their coupling with the lattice vibrations. In contrast to the case of electron-phonon coupling, where phonons can be disregarded at low temperatures, the magnon dispersion may undergo significant changes with new states emerging in the band gap [45,46]. We find that in the honeycomb ferromagnet with spins oriented orthogonal to the lattice plane, only transverse phonon modes with out-of-plane displacement couple to spin. To understand the eigenmodes, we evaluate and analyze the coupled spin and out-of-plane phonon modes for an infinitely large plane as well as for a finite ribbon geometry. We quantify the effect of the magnetoelastic coupling on the magnon Hall conductivity and find a nonmonotonic dependence on the coupling strength. Our analysis of the finite ribbons shows that topological magnons hybridize with bulk phonons around the avoided crossings in their coupled dispersion, forming magnon polarons with topological chiral properties. Hence, while their edge localization is weakened, the magnetoelastic coupling does not completely remove the topological magnons. Furthermore, we find that armchair edges support Rayleigh-like edge phonon modes in sharp contrast to the zigzag edges. When topological magnons hybridize with these edge phonons, edge magnon polarons with almost undiminished chirality are formed. We suggest a setup that utilizes this induced chirality in coherent phonon transport. Such systems enable the observation of the topological physics and serve as a prototype for a unidirectional heat pump. This offers a highly feasible alternative to producing topological phonon diodes [47–49].

Model.—We consider a ferromagnetic material with localized spins on a two-dimensional honeycomb lattice, allow for out-of-plane vibrations of the lattice sites, and

assume there is magnetoelastic coupling. This system can be modelled by a Hamiltonian of the form $H = H_m + H_{\rm ph} + H_{\rm me}$, where H_m is the magnetic Hamiltonian, $H_{\rm ph}$ describes the phonons, and $H_{\rm me}$ represents the magnetoelastic coupling.

The Hamiltonian we consider is inspired by the Haldane model [1], and given by [15–17]

$$H_m = -J\sum_{\langle i,j\rangle}\mathbf{S}_i\cdot\mathbf{S}_j + \mathcal{D}\sum_{\langle\langle i,j\rangle\rangle}\nu_{ij}\hat{z}\cdot\mathbf{S}_i\times\mathbf{S}_j - \mathcal{B}\sum_i S_i^z. \quad (1)$$

The first term describes the ferromagnetic exchange coupling between nearest neighbor sites, while the second accounts for the Dzyaloshinskii-Moriya interaction [20,21] between next-to-nearest neighbors [50]. The Haldane sign $\nu_{ij} = \pm 1$ depends on the relative orientation of the next-to-nearest neighbors as shown in Fig. 1(a), and is the root of nontrivial topological properties. We let the nearest neighbor distance be d and the next-to-nearest neighbor distance be a. References [16,17] discuss the dispersion relation and Berry curvature of this spin model in linear spin wave theory.

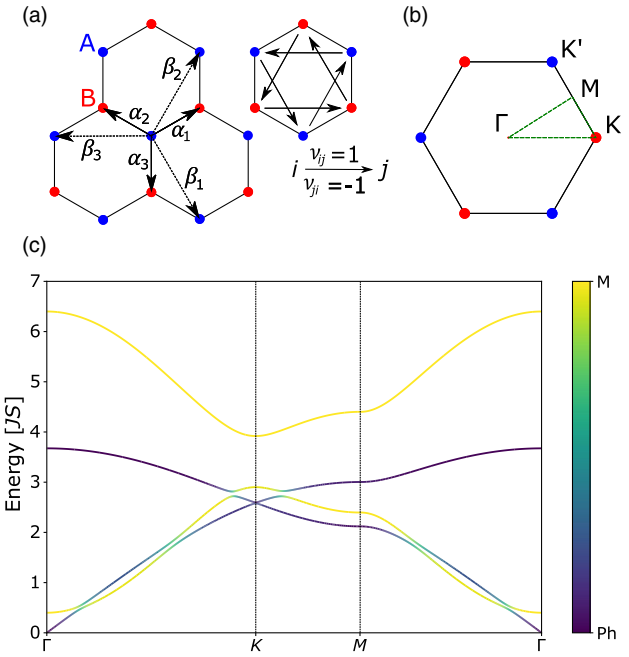

FIG. 1. (a) Lattice geometry showing the nearest neighbor vectors $\boldsymbol{\alpha}$, next-to-nearest neighbor vectors $\boldsymbol{\beta}$, and the Haldane sign $\nu_{ij} = \pm 1$. (b) The first Brillouin zone in reciprocal space, including the paths along which we plot the dispersion relation in (c). The parameter values used are $\mathcal{D} = 0.1J$, $\mathcal{B} = 0.4JS$, $\sqrt{C/m} = 1.5JS$, and rescaled coupling strength $\tilde{\kappa} = 0.03$ (see main text). The magnon (yellow) and phonon (purple) character of the modes is indicated with colors. The modes are significantly affected by the magnetoelastic coupling only close to avoided crossings.

For the phonon Hamiltonian, we consider only the out-of-plane degrees of freedom since only these modes couple to the spin to lowest order in the linear spin wave expansion. We assume nearest-neighbor interactions with elastic constant C, let the mass associated with the spins on the lattice sites be m, and disregard substrate coupling. Introducing $S_k = \sum_\beta \cos(\mathbf{k}\cdot\boldsymbol{\beta})$, where the sum is over the three next-to-nearest neighbor vectors $\boldsymbol{\beta}$ of Fig. 1(a), we obtain the dispersion relation

$$\omega_\pm^{\rm ph}(\mathbf{k}) = \sqrt{\frac{C}{m}}\sqrt{3 \pm \sqrt{3+2S_k}} \quad (2)$$

for the free phonon modes.

Motivated by the continuum limit description [36,37], we write down the lattice magnetoelastic coupling to linear order in the magnon amplitude, obtaining

$$H_{\rm me} = \kappa\sum_D\sum_{i\in D}\sum_{\boldsymbol{\alpha}_D}\mathbf{S}_i\cdot\boldsymbol{\alpha}_D(u_i^z - u_{i+\boldsymbol{\alpha}_D}^z), \quad (3)$$

where κ parametrizes the strength of the magnon-phonon coupling, $\sum_D$ denotes the sum over sublattices, $\sum_{i\in D}$ is the sum over the lattice sites on the D sublattice, and $\boldsymbol{\alpha}_D$ are the corresponding nearest neighbor vectors. The out-of-plane deviation for lattice site i is denoted by u_i^z.

Bulk spectrum.—We introduce the Holstein-Primakoff representation of spins and use linear spin wave theory in the spin- and magnetoelastic terms [27]. Within the rotating wave approximation [51], the resulting Hamiltonian describing the phonon and magnon modes of the system is obtained as $H = \sum_k \psi_k^\dagger M_k \psi_k$, where $\psi_k^\dagger = (a_k^\dagger, b_k^\dagger, c_{k-}^\dagger, c_{k+}^\dagger)$. Here, a_k and b_k are annihilation operators for the sublattice magnon modes on the A and B sublattices, while $c_{k\pm}$ are the annihilation operators for the phonon modes. The matrix M_k takes the form

$$M_k = \begin{pmatrix} A + h^z & h^- & g_{A-} & g_{A+} \\ h^+ & A - h^z & g_{B-} & g_{B+} \\ g_{A-}^* & g_{B-}^* & \omega_{k-}^{\rm ph} & 0 \\ g_{A+}^* & g_{B+}^* & 0 & \omega_{k+}^{\rm ph} \end{pmatrix}, \quad (4)$$

where $A = 3JS + \mathcal{B}$, $h^z(\mathbf{k}) = 2\mathcal{D}S\sum_\beta \sin(\mathbf{k}\cdot\boldsymbol{\beta})$, $h^-(\mathbf{k}) = -JS\sum_\alpha \exp(-i\mathbf{k}\cdot\boldsymbol{\alpha})$, and $h^+ = (h^-)^*$. The coupling between the D-sublattice magnons and the phonon branch $\pm$ is captured by $g_{D\pm}$, which is proportional to the dimensionless coupling strength $\tilde{\kappa} = (\kappa d/JS) \times \sqrt[4]{\hbar^2 S^2/16m^2(C/m)}$. The spectrum obtained by diagonalizing this matrix is plotted in Fig. 1(c) along the paths displayed in Fig. 1(b).

Hall conductivity.—The topological nature of the spin model is manifested in the magnon Hall conductivity that

arises because of the time-reversal symmetry breaking caused by the Dzyaloshinskii-Moriya interaction.

The spin current operator J_γ may be found from a continuity equation or magnon group velocity approach [52], both yielding

$$J_\gamma = \sum_k \begin{pmatrix} a_k^\dagger & b_k^\dagger \end{pmatrix} \left(\frac{\partial H_m(\mathbf{k})}{\partial k_\gamma} \right) \begin{pmatrix} a_k \\ b_k \end{pmatrix} \tag{5}$$

along the Cartesian direction γ. Here, $H_m(\mathbf{k})$ is the matrix representation of the magnon Hamiltonian. Assuming we apply a weak in-plane magnetic field gradient $\nabla\mathcal{B}$, we are interested in the current $\mathbf{j} = \sigma\nabla\mathcal{B}$, which is determined by the conductivity tensor σ [52]. The Hall conductivity can be calculated using the Kubo formula, giving

$$\sigma_{xy} = \sum_k \sum_{\alpha,\beta\neq\alpha} n_B(E_{k\alpha}) C_{\alpha\beta}(\mathbf{k}), \tag{6}$$

where $E_{k\alpha}$ is the energy eigenvalue of band α and $n_B(E_{k\alpha})$ is the corresponding Bose factor. The curvature tensor $C_{\alpha\beta}$ is given by

$$C_{\alpha\beta}(\mathbf{k}) = i \frac{J_y^{\alpha\beta}(\mathbf{k}) J_x^{\beta\alpha}(\mathbf{k}) - J_x^{\alpha\beta}(\mathbf{k}) J_y^{\beta\alpha}(\mathbf{k})}{(E_{k\alpha} - E_{k\beta})^2}, \tag{7}$$

where (α, β) are band indices, and $J_\gamma^{\alpha\beta}(\mathbf{k})$ are the energy eigenstate matrix elements of the current operator at quasimomentum $\mathbf{k}$. Disregarding the magnetoelastic coupling, the band curvature $C_\alpha = \sum_{\beta\neq\alpha} C_{\alpha\beta}$ can be identified as the Berry curvature.

Expressing the sublattice magnon operators in terms of the eigenmode operators, one may identify the current matrix elements $J_\gamma^{\alpha\beta}$ and integrate the curvature over the Brillouin zone to obtain the Hall conductivity. We are particularly interested in the effect of the magnetoelastic coupling, and therefore present the dependence of the Hall conductivity on the dimensionless coupling $\tilde{\kappa}$ in Fig 2.

To understand this dependence, we consider the curvature tensor $C_{\alpha\beta}$. When the bands α and β both have a predominant magnon content, the topological nature of the underlying magnons gives a finite curvature. This magnon curvature is largest close to the Dirac points [16,17]. Close to an avoided crossing, the magnetoelastic coupling changes the spectrum and causes transfer of band curvature between the relevant bands α and β. The latter can be seen by plotting the curvature tensor element $C_{\alpha\beta}$ for the band pairs with avoided crossings, as shown in the insets of Fig 2. The resulting change in Hall conductivity is given by these curvature tensor elements weighted with the difference between the Bose factors of the relevant bands. This follows from the antisymmetry property of the curvature tensor. The two band pairs in the insets contribute oppositely to the Hall conductivity, and the competition between their curvature transfer explains the nonmonotonic behavior of the Hall conductivity.

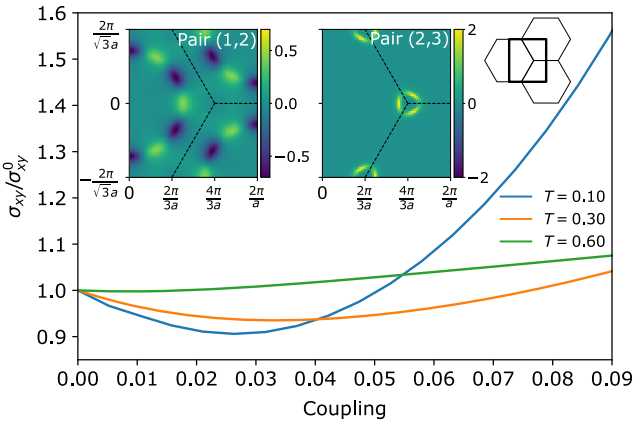

FIG. 2. Dependence of the Hall conductivity on the magnetoelastic coupling strength $\tilde{\kappa}$ for parameter values $\mathcal{D} = 0.1J$, $\mathcal{B} = 0.4JS$, and $\sqrt{C/m} = 1.5JS$ for different temperatures T in units of JS. The insets show the quasimomentum dependence of the curvature tensor at $\tilde{\kappa} = 0.03$ for band pairs (1,2) and (2,3), where the bands are labeled according to their energy, and band 1 is the lowest band. The dominant contribution in these band pairs comes from the regions with avoided crossings of the respective bands.

Ribbon geometry and coherent transport.—Due to the topological nature of the magnon model under consideration and the bulk-boundary correspondence, there are gapless magnon edge states in a finite sample [5,15–17]. Considering an armchair ribbon with finite width, the one-dimensional projection of the energy spectrum is plotted in Fig. 3. The corresponding spectrum for the zigzag edge ribbon is given in the Supplemental Material [53], where also Refs. [54–58] appear. Magnon and phonon modes hybridize in regions with an avoided crossing. When the upper phonon band lies within the band gap of the pure magnon spectrum, there are modes with a mixed content of chiral magnon edge states and phonons. Although the spectra look qualitatively similar, there is a crucial distinction between the two cases. For the zigzag edge configuration, all the phonon modes are delocalized throughout the sample, while the armchair edges host "Rayleigh-like" edge phonon modes. In direct analogy with Rayleigh modes on the surface of a three-dimensional material, the localization length of these modes is directly proportional to their wavelength, as shown in the Supplemental Material [53]. These edge phonon modes are supported by the half-hexagon protrusions of the armchair edge that can pivot around the bonds parallel to the edges connecting these protrusions, see Fig. 3. No such parallel bonds exist for the zigzag edge.

The Hall conductivity is a hallmark of topological electronic properties and motivates a similar role for the Hall conductivity mediated by topological magnons. However,

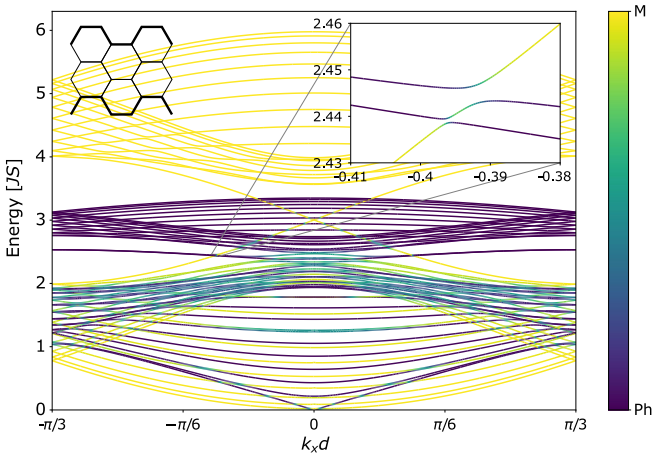

FIG. 3. One-dimensional projection of the dispersion relation for the magnetoelastic modes on a honeycomb ribbon with armchair edges. In addition to the bulk bands, there are two topological edge magnon states crossing the magnon band gap, as well as Rayleigh-like edge phonons. The inset shows the avoided crossing of a topological magnon edge mode with the two quasidegenerate edge phonon modes. The parameter values are $\mathcal{B} = 0$, $\sqrt{C/m} = 1.37JS$, $\mathcal{D} = 0.1J$, and $\tilde{\kappa} = 0.03$.

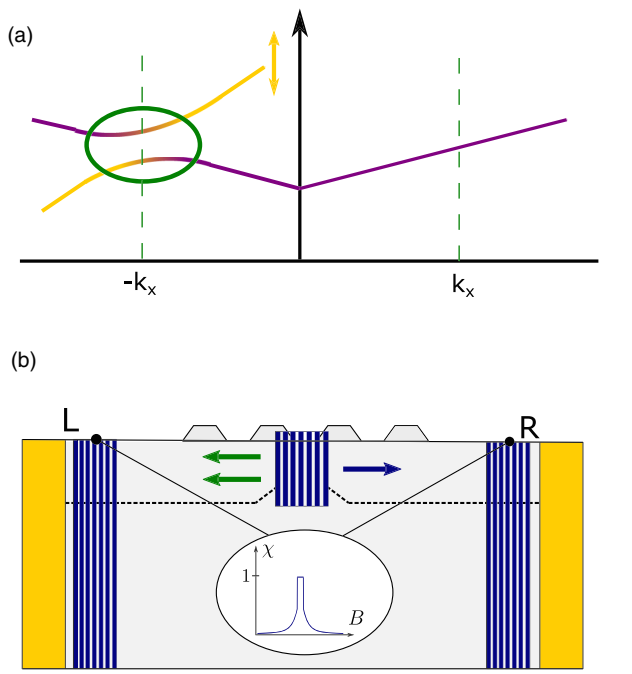

FIG. 4. (a) Schematic spectrum for the coupled Rayleigh-like edge phonons and the topological edge magnon on the upper armchair sample edge. The phonon at quasimomentum $-k_x$ hybridizes with the chiral magnon, while the phonon at quasimomentum $+k_x$ is unaffected due to the lack of a magnon with a matching wave vector at this edge. At the avoided crossing, there is propagation direction reversal for the modes with a phononic content. The color of the dispersion represents its nature with purple representing phononic and yellow magnonic character. (b) Proposed experimental setup for detecting coherent chiral transport through excitation of phononic modes. Elastic energy is injected in the sample middle on the upper armchair edge and detected at the left (L) and right (R) edges using wave vector and frequency resolved elastic transducers (purple). By exciting modes at the avoided crossing in (a), only the elastic excitations at one of the two quasimomenta $\pm k_x$ are converted into hybridized modes (green arrows). This gives a chiral response, and the chirality is peaked when the wave vector of the avoided crossing coincides with the fixed wave vector of the transducer.

in contrast to electrons, the bosonic nature of the magnons results in the lack of a general proportionality between the magnon Hall conductivity and the Chern number [52]. Furthermore, the observation of a magnon planar Hall effect [59] in a cubic, nontopological magnet suggests that this Hall conductivity may not be regarded as a smoking-gun signature for topological properties. Thus, we suggest a complementary approach to observe the topological nature of the underlying magnons by elastically probing the chirality of the magnetoelastic hybrid modes.

We propose to observe coherent chiral phonon propagation in the experimental setup of Fig. 4(b) by utilizing the edge modes, as depicted schematically in Fig. 4(a) [60], on the upper armchair edge of the sample. Taking inspiration from previous related experiments [41,61], we suggest injecting elastic energy into the sample middle at the upper edge using a nanoscale variant of the interdigital transducer design [62,63], elaborated further in the Supplemental Material [53]. For a given transducer design, modes are excited with fixed wave vectors $\pm k_x$ and a tunable frequency. Similar transducers can be used to detect the elastic response $p_{L/R}$ on the left (L) and right (R) edges of the sample. Here, $p_{L/R}$ is the elastic power detected at the transducers.

Figure 4(a) schematically depicts the dispersion for the magnetoelastic modes localized on an armchair edge. Disregarding magnetoelastic coupling, the edge hosts two counterpropagating Rayleigh-like edge phonons and a single chiral edge magnon. There is thus no chirality in the phononic response. Due to magnetoelastic coupling, the Rayleigh-like phonon with wave vector $-k_x$ hybridizes with the chiral magnon to form a magnon polaron while the other phonon remains unchanged. This breaks the symmetry between the counterpropagating phononic modes and the result is nonzero chirality $\chi = (p_R - p_L)/(p_R + p_L)$. Furthermore, as shown in Fig. 4(a), the hybridization with the magnon mode reverses the group velocity direction of the participating phonon mode. In principle, this gives perfectly chiral phonon transport.

The wave vector location of the avoided crossing can be tuned via the Zeeman shift in the magnon dispersion. Performing a frequency integrated measurement over an energy range of the same order as the magnetoelastic coupling, one obtains a peaked chirality when the magnetic field is such that the wave vector of the avoided crossing coincides with the wave vector of the transducer, obtaining

a chirality as shown in Fig. 4(b). Performing a similar transport experiment on the zigzag edge does not give chiral phonon transport since the delocalized phonons hybridize with counterpropagating magnons on both the edges, thereby destroying the overall chirality. In addition, the size of the avoided crossing is smaller due to the smaller overlap with the localized chiral magnon. The armchair edge is therefore crucial for obtaining the chirality.

Summary.—We have examined the robustness of topological magnons in a honeycomb ferromagnet against their interaction with phonons. Their topological properties, albeit weakened, survive the magnetoelastic coupling. The magnon Hall conductivity of the system is found to depend on the magnetoelastic coupling strength in a nonmonotonic, temperature-sensitive manner. Exploiting the Rayleigh-like edge phonons in armchair ribbons, we predict the existence of topological magnon polarons confined to the boundary. We have suggested an experimental setup capable of probing the chiral nature of the topological magnon polarons by elastic means, which thus serves as a platform for chiral coherent phononic transport.

We acknowledge support from the Research Council of Norway Grant No. 262633 "Center of Excellence on Quantum Spintronics," and No. 250985, "Fundamentals of Low-dissipative Topological Matter."

*asle.sudbo@ntnu.no

[1] F. D. M. Haldane, Model for a Quantum Hall Effect without Landau Levels: Condensed-Matter Realization of the "Parity Anomaly", Phys. Rev. Lett. **61**, 2015 (1988).
[2] C. L. Kane and E. J. Mele, Z_2 Topological Order and the Quantum Spin Hall Effect, Phys. Rev. Lett. **95**, 146802 (2005).
[3] C. L. Kane and E. J. Mele, Quantum Spin Hall Effect in Graphene, Phys. Rev. Lett. **95**, 226801 (2005).
[4] B. Bernevig, T. L. Hughes, and S.-C. Zhang, Quantum spin hall insulator state in hgte quantum wells, Science **314**, 1757 (2006).
[5] M. Z. Hasan and C. L. Kane, Colloqium: Topological Insulators, Rev. Mod. Phys. **82**, 3045 (2010).
[6] C. W. J. Beenakker, Search for majorana fermions in superconductors, Annu. Rev. Condens. Matter Phys. **4**, 113 (2013).
[7] J. Alicea, New directions in the pursuit of majorana fermions in solid state systems, Rep. Prog. Phys. **75**, 076501 (2012).
[8] V. Mourik, K. Zuo, S. M. Frolov, S. R. Plissard, E. P. A. M. Bakkers, and L. P. Kouwenhoven, Signatures of majorana fermions in hybrid superconductor-semiconductor nanowire devices, Science **336**, 1003 (2012).
[9] L. Fu and C. L. Kane, Superconducting Proximity Effect and Majorana Fermions at the Surface of a Topological Insulator, Phys. Rev. Lett. **100**, 096407 (2008).
[10] C. Nayak, S. H. Simon, A. Stern, M. Freedman, and S. Das Sarma, Non-abelian anyons and topological quantum computation, Rev. Mod. Phys. **80**, 1083 (2008).
[11] S. Das Sarma, M. Freedman, and C. Nayak, Topologically Protected Qubits from a Possible Non-Abelian Fractional Quantum Hall State, Phys. Rev. Lett. **94**, 166802 (2005).
[12] G. Jotzu, M. Messer, R. Desbuquois, M. Lebrat, T. Uehlinger, D. Greif, and T. Esslinger, Experimental realization of the topological haldane model with ultracold fermions, Nature (London) **515**, 237 (2014).
[13] S. Lannebère and M. G. Silveirinha, Link between the photonic and electronic topological phases in artificial graphene, Phys. Rev. B **97**, 165128 (2018).
[14] Y. Liu, Y. Xu, S.-C. Zhang, and W. Duan, Model for topological phononics and phonon diode, Phys. Rev. B **96**, 064106 (2017).
[15] S. A. Owerre, A first theoretical realization of honeycomb topological magnon insulator, J. Phys. Condens. Matter **28**, 386001 (2016).
[16] S. A. Owerre, Topological honeycomb magnon hall effect: A calculation of thermal hall conductivity of magnetic spin excitations, J. Appl. Phys. **120**, 043903 (2016).
[17] S. K. Kim, H. Ochoa, R. Zarzuela, and Y. Tserkovnyak, Realization of the Haldane-Kane-Mele Model in a System of Localized Spins, Phys. Rev. Lett. **117**, 227201 (2016).
[18] S. A. Owerre and J. Nsofini, Squeezed dirac and topological magnons in a bosonic honeycomb optical lattice, J. Phys. Condens. Matter **29**, 455802 (2017).
[19] H.-S. Kim and H.-Y. Kee, Realizing haldane model in fe-based honeycomb ferromagnetic insulators, npj Quantum Mater. **2**, 20 (2017).
[20] I. Dzyaloshinsky, A thermodynamic theory of weak ferromagnetism of antiferromagnetics, J. Phys. Chem. Solids **4**, 241 (1958).
[21] T. Moriya, Anisotropic superexchange interaction and weak ferromagnetism, Phys. Rev. **120**, 91 (1960).
[22] A. Rückriegel, A. Brataas, and R. A. Duine, Bulk and edge spin transport in topological magnon insulators, Phys. Rev. B **97**, 081106 (2018).
[23] V. V. Kruglyak, S. O. Demokritov, and D. Grundler, Magnonics, J. Phys. D **43**, 264001 (2010).
[24] A. V. Chumak, V. I. Vasyuchka, A. A. Serga, and B. Hillebrands, Magnon spintronics, Nat. Phys. **11**, 453 (2015).
[25] G. E. W. Bauer, E. Saitoh, and B. J. van Wees, Spin caloritronics, Nat. Mater. **11**, 391 (2012).
[26] K. Uchida, J. Xiao, H. Adachi, J. Ohe, S. Takahashi, J. Ieda, T. Ota, Y. Kajiwara, H. Umezawa, H. Kawai, G. E. W. Bauer, S. Maekawa, and E. Saitoh, Spin seebeck insulator, Nat. Mater. **9**, 894 (2010).
[27] A. I. Akhiezer, V. G. Bar'iakhtar, and S. V. Peletminski, *Spin Waves* (North-Holland Publishing Company, Amsterdam, 1968).
[28] A. V. Chumak, A. A. Serga, and B. Hillebrands, Magnon transistor for all-magnon data processing, Nat. Commun. **5**, 4700 (2014).
[29] K. Ganzhorn, S. Klingler, T. Wimmer, S. Geprgs, R. Gross, H. Huebl, and S. T. B. Goennenwein, Magnon-based logic in a multi-terminal yig/pt nanostructure, Appl. Phys. Lett. **109**, 022405 (2016).
[30] T. An, V. I. Vasyuchka, K. Uchida, A. V. Chumak, K. Yamaguchi, K. Harii, J. Ohe, M. B. Jungfleisch, Y. Kajiwara, H. Adachi, B. Hillebrands, S. Maekawa,

and E. Saitoh, Unidirectional spin-wave heat conveyer, Nat. Mater. **12**, 549 (2013).
[31] E. Saitoh, M. Ueda, H. Miyajima, and G. Tatara, Conversion of spin current into charge current at room temperature: Inverse spin-hall effect, Appl. Phys. Lett. **88**, 182509 (2006).
[32] E. B. Sonin, Spin currents and spin superfluidity, Adv. Phys. **59**, 181 (2010).
[33] S. Takei, B. I. Halperin, A. Yacoby, and Y. Tserkovnyak, Superfluid spin transport through antiferromagnetic insulators, Phys. Rev. B **90**, 094408 (2014).
[34] A. Kamra and W. Belzig, Super-Poissonian Shot Noise of Squeezed-Magnon Mediated Spin Transport, Phys. Rev. Lett. **116**, 146601 (2016).
[35] A. Kamra, U. Agrawal, and W. Belzig, Noninteger-spin magnonic excitations in untextured magnets, Phys. Rev. B **96**, 020411 (2017).
[36] C. Kittel, Physical theory of ferromagnetic domains, Rev. Mod. Phys. **21**, 541 (1949).
[37] C. Kittel, Interaction of spin waves and ultrasonic waves in ferromagnetic crystals, Phys. Rev. **110**, 836 (1958).
[38] K. Uchida, H. Adachi, T. An, T. Ota, M. Toda, B. Hillebrands, S. Maekawa, and E. Saitoh, Long-range spin seebeck effect and acoustic spinpumping, Nat. Mater. **10**, 737 (2011).
[39] A. Kamra, H. Keshtgar, P. Yan, and G. E. W. Bauer, Coherent elastic excitation of spin waves, Phys. Rev. B **91**, 104409 (2015).
[40] A. Kamra and G. E. W. Bauer, Actuation, propagation, and detection of transverse magnetoelastic waves in ferromagnets, Solid State Commun. **198**, 35 (2014).
[41] M. Weiler, H. Huebl, F. S. Goerg, F. D. Czeschka, R. Gross, and S. T. B. Goennenwein, Spin Pumping with Coherent Elastic Waves, Phys. Rev. Lett. **108**, 176601 (2012).
[42] L. Dreher, M. Weiler, M. Pernpeintner, H. Huebl, R. Gross, M. S. Brandt, and S. T. B. Goennenwein, Surface acoustic wave driven ferromagnetic resonance in nickel thin films: Theory and experiment, Phys. Rev. B **86**, 134415 (2012).
[43] B. Flebus, K. Shen, T. Kikkawa, K.-i. Uchida, Z. Qiu, E. Saitoh, R. A. Duine, and G. E. W. Bauer, Magnon-polaron transport in magnetic insulators, Phys. Rev. B **95**, 144420 (2017).
[44] T. Kikkawa, K. Shen, B. Flebus, R. A. Duine, K.-i. Uchida, Z. Qiu, G. E. W. Bauer, and E. Saitoh, Magnon Polarons in the Spin Seebeck Effect, Phys. Rev. Lett. **117**, 207203 (2016).
[45] D. A. Bozhko, P. Clausen, G. A. Melkov, V. S. L'vov, A. Pomyalov, V. I. Vasyuchka, A. V. Chumak, B. Hillebrands, and A. A. Serga, Bottleneck Accumulation of Hybrid Magnetoelastic Bosons, Phys. Rev. Lett. **118**, 237201 (2017).
[46] A. Rückriegel, P. Kopietz, D. A. Bozhko, A. A. Serga, and B. Hillebrands, Magnetoelastic modes and lifetime of magnons in thin yttrium iron garnet films, Phys. Rev. B **89**, 184413 (2014).
[47] N. Li, J. Ren, L. Wang, G. Zhang, P. Hänggi, and B. Li, Colloqium: Phononics: Manipulating heat flow with electronic analogs and beyond, Rev. Mod. Phys. **84**, 1045 (2012).
[48] M. Maldovan, Sound and heat revolutions in phononics, Nature (London) **503**, 209 (2013).
[49] Y. Liu, Y. Xu, S.-C. Zhang, and W. Duan, Model for topological phononics and phonon diode, Phys. Rev. B **96**, 064106 (2017).
[50] The demagnetization energy is disregarded since it only causes minor shifts in the dispersion [35].
[51] M. O. Scully and M. S. Zubairy, *Quantum Optics* (Cambridge University Press, Cambridge, 1997).
[52] K. Nakata, J. Klinovaja, and D. Loss, Magnonic quantum hall effect and wiedemann-franz law, Phys. Rev. B **95**, 125429 (2017).
[53] See Supplemental Material at http://link.aps.org/supplemental/10.1103/PhysRevLett.122.107201 for details of the derivation of the main results of the paper.
[54] C. Kittel, *Quantum Theory of Solids* (John Wiley & Sons, New York, 1987).
[55] G. S. Kino, *Acoustic Waves: Devices, Imaging, and Analog Signal Processing*, Prentice-Hall Contemporary Topics in Accounting Series (Prentice-Hall, Englewood Cliffs, New Jersey, 1987).
[56] A. A. Maradudin and G. I Stegeman, Surface Acoustic Waves, in *Surface Phonons*, edited by F. W. de Wette and W. Kress (Springer-Verlag, Berlin-Heidelberg, 1991), Chap. 2, pp. 5–36.
[57] B. Andrei Bernevig and T. L. Hughes, *Topological Insulators and Topological Superconductors* (Princeton University Press, Princeton, New Jersey, 2013).
[58] P. Ruello and V. E. Gusev, Physical mechanisms of coherent acoustic phonons generation by ultrafast laser action, Ultrasonics **56**, 21 (2015).
[59] J. Liu, L. J. Cornelissen, J. Shan, T. Kuschel, and B. J. van Wees, Magnon planar hall effect and anisotropic magnetoresistance in a magnetic insulator, Phys. Rev. B **95**, 140402 (2017).
[60] The inset of Fig. 3(b) shows two phonon modes. One is irrelevant since it is localized on the opposite edge.
[61] P. G. Gowtham, T. Moriyama, D. C. Ralph, and R. A. Buhrman, Traveling surface spin-wave resonance spectroscopy using surface acoustic waves, J. Appl. Phys. **118**, 233910 (2015).
[62] S. Datta, *Surface Acoustic Wave Devices* (Prentice-Hall, Englewood Cliffs, New Jersey, 1986).
[63] A. V. Mamishev, K. Sundara-Rajan, Fumin Yang, Yanqing Du, and M. Zahn, Interdigital sensors and transducers, Proc. IEEE **92**, 808 (2004).